ISSN (Print) 1226-1750
ISSN (Online) 2233-6656
Journal of Magnetics 18(1), 50-56 (2013) http://dx.doi.org/10.4283/JMAG.2013.18.1.050

Comparative Analysis of Flux-Reversal Motors with Six-Switch and Four-Switch Converters

Hyun-Soo Kang[1], Byoung-Kuk Lee[2], and Tae Heoung Kim[3]*

[1]*ADT Co. Ltd, 984-3 Kwanyang-dong, Anyang-si, Gyeonggi 431-060, Korea*
[2]*School of Information and Communication Engineering, Sungkyunkwan University, Suwon 440-746, Korea*
[3]*Department of Electrical Engineering, Engineering Research Institute, Gyeongsang National University, Gyeongnam 660-701, Korea*

(Received 10 December 2012, Received in final form 5 February 2013, Accepted 13 February 2013)

In this paper, the 6-switch inverter for the Flux-Reversal Motor (FRM) has been presented and compared to the 4-switch inverter for the FRM, which is more popular in cost effective applications. To analyze the FRM, we adopted the two-dimensional time-stepped voltage source finite element method (FEM) that uses the actual pulse width modulation (PWM) voltage waveforms as the input data. As the FRM characteristic analysis of actual pwm voltage input, the torque ripples and iron losses (eddy current and hysteresis loss) of the FRM can be precisely calculated. With the simulated and experimental results, the performance and limitations of the 4-switch FRM which is the cost effective drive compared to the 6-switch FRM drive are provided in more detail.

Keywords : flux-reversal machine, finite element method, 4-switch

1. Introduction

Among of many ac motors, the induction machine (IM) has been regarded as the most popular one and has dominated various areas. Therefore, there are many studies and topologies in the IM applications. However, in the case of the permanent magnet motor (PMM), with high efficiency, high power factor, high torque, simple control, and lower maintenance, compared to the IM, it has replaced the conventional dc motors and IMs [1, 2]. Although the switched reluctance motor (SRM) has gained much interest in recent years due to its advantages, such as its simple structure and high power density due to high speed, it has some restrictions, such as complex drive circuitry, inherent peak torque ripple, and control complexity. The SRM is always a popular machine for high speed operation due to its very simple and robust rotor construction. Unfortunately, a reasonable electromagnetic design could not be achieved without reducing the clearance gap considerably below the required value which is described in many papers. Furthermore, in order to achieve a reasonable efficiency, 0.178 mm (0.007 in) thick laminations were required in both the stator and the rotor [3]. Also, in SRM it exhibits comparatively high windage losses due to the salient pole rotor structure and it is also difficult to maintain the tightness of the rotor laminations to avoid mechanical variation of the rotor at high speeds. Compared to these SRM characteristics, the interior-type PMM has higher efficiency and torque per volume than the surface-type PMM and it has expanded its regions to various commercial, industrial, and transportation applications. For example, the areas of interior-type PMM are electric vehicles, spindle drives, compressors, and so on due to its high efficiency and wide speed range [4, 5]. However, using a permanent magnet on the rotor, the surface-type PMM causes severe limitation on high speed operations. The usual method is to use high-energy sintered magnets held against the shaft by a shrunk-on metallic shell or a fiber wrap. Due to this characteristic the interior-type PMM is preferred for use in high speed applications but it produces significant cogging torque which generates vibration and noise. Also, by using the interior-type PMM, a complex algorithm is needed for the reluctance torque component as well as magnetic torque component. Under this background, researchers have attempted to combine the merits of SRM and PMM, leading to propose a new machine structure as Flux Reversal Motor (FRM), which has a simple structure and low rotor inertia, for low cost and high speed applications [6].

*Corresponding author: Tel: +82-55-772-1717
Fax: +82-55-772-1719, e-mail: ktheoung@gnu.ac.kr

In fact, the FRM is not the unique combining machine that has the stationary magnets and simple reluctance rotor, it has a very strong configuration compared to the other permanent magnet machines and it appears that the type of FRM has a naturally low inductance and consequently it has a low electrical time constant compared to other PMMs. There are some researches about the FRM drive itself. For example, in [7], it introduces the pwm mode for the control of the FRM drive and the influences on the performance of the FRM drive is analyzed through FEM. In [8], the dynamic characteristics of the FRM drive under different pwm modes are presented and in case of the input current, the sine-wave and rectangular-wave currents are compared, and finally the torque ripple and iron losses are analyzed for the economic point of view. Also in [9], the FRM is modeled for the iron losses comparison in different pwm mode; as a result the PWM-ON mode has the merit in terms of iron loss in the conventional 6-switch inverter.

The FRM requires quasi-square current waveforms, usually synchronized with the back-EMF to generate constant output torque and have 120 degree conduction and 60 degree non-conducting regions similar to brushless dc machines. Also, at every instant only two phases are conducting and the other phase is inactive. This control method can be realized using the conventional 6-switch inverter topology as shown in Fig. 1(a). For the purpose of cost reduction, from the conventional 6-switch configuration, one switch leg is redundant to drive 3-phase FRM, resulting in the possibility of the 4-switch configuration as shown in Fig. 1(b). Also, from a software point of view, a simple control scheme, direct current controlled pulse width modulation (PWM), is suitable for the cost effective 4-switch FRM [10, 11]. From an economic point of view, it can be a good machine-drive combination in the use of the FRM and 4-switch inverter because both elements of the system reduced the control complexity and the manufactured cost. In addition to this point of view, these motor and drive combinations are a good solution to high speed applications, for example compressor drives. With rectangular current input that causes lower switching frequencies compared to interior-type PMM or surface-type PMM which has sinusoidal current input per phase, FRM has considerably less switching losses and smaller heatsink size. These mechanical combinations result in compact volume and the FRM has a rotor which does not need to retain the rotor magnet at high speed. However, due to supplying voltage irregularity and lack of a phase control freedom, the phase current can fluctuate much more. Therefore, it is necessary to analyze the overall performance with respect to torque

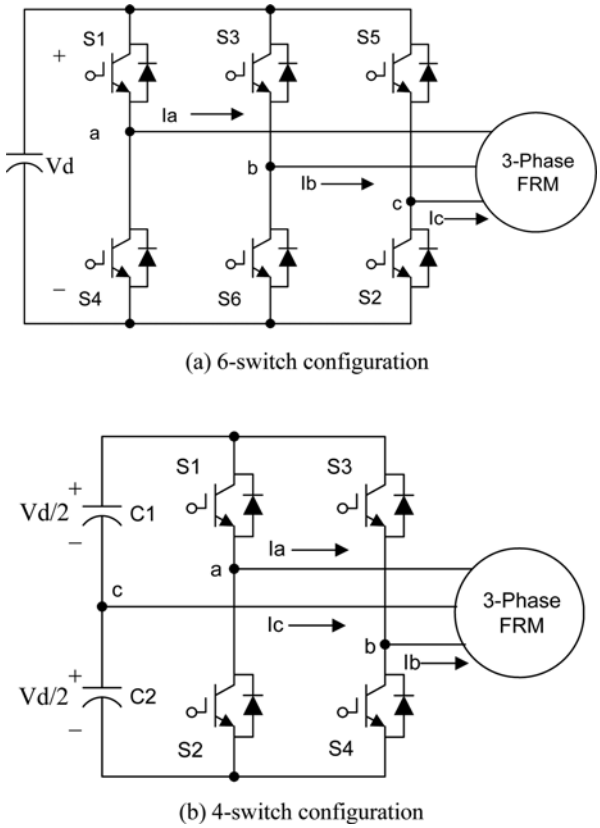

Fig. 1. Configuration of the 6-switch and 4-switch FRM.

pulsation, eddy current and hysteresis losses in the 4-switch FRM drive for a certain application compared to 6-switch conventional drives.

In this paper, we adopted the two-dimensional time-stepped voltage source finite element method (FEM), which uses the actual pwm voltage waveforms of 6-switch and 4-switch drives as the input data and is coupled with the equations of pwm drive circuits. Based on this FEM, the characteristic analysis of FRM with different power conversion topologies is presented in detail. A 100W rated FRM has been designed and manufactured and 6-switch and 4-switch drive test-beds are implemented to examine the overall performance comparison.

2. Analysis of 4-Switch Flux Reversal Motor and Drives Characteristics

2.1. 4-Switch pwm Drive Algorithm for Flux Reversal Motor

As the 4-switch inverter for the FRM drive is similar to the permanent magnet brushless machine 4-switch drive, the three-phase currents should be synchronized with each counterpart back-EMF, so that the overall operation can be divided into six modes. The quasi-square current

waveforms inputs flow into the FRM, which are synchronized with the back-EMF to generate constant output torque and have 120 degree conduction and 60 degree non-conducting regions. For the view point of the cost reduction, usually at the 6-switch VSI, one of the three legs is redundant to drive three-phase FRM, since one phase of the machine is always connected to the neutral of the dc-link capacitors, i.e. if phase A and B currents are controllable in a conduction regions, the other phase C is uncontrollable in a non-conduction region. Compared to the conventional 6-switch inverter for the FRM drive, in case of the 4-switch FRM drive, the inverter can only generate four switching vectors, such as (0,0), (0,1), (1,0), and (1,1), where "0" means that the lower switch is turned on and "1" the upper switch is turned on. With these four switching vectors, it is difficult to generate the proper current waveforms as the non-conduction region has not zero-current because the neutral point of the capacitor has some potential voltage in actual status. For example, in case that current flows through phase A and B, the back-EMF of phase C should be blocked to ensure there is no current in phase C. Therefore, the 4-switch drive with the direct current controlled pwm method [10], phase A and phase B currents should be sensed and controlled independently and the switching signals of S1 (S3) and S2 (S4) should be created independently. Therefore, in this paper, the direct current controlled PWM algorithm has been applied to generate speed-torque characteristics.

The actual phase currents are controlled by a hysteresis current controller or digital PI current controller with two phase current sensing, phase A and phase B. In order to examine the performance of the 4-switch FRM drive using the finite element method, the detailed voltage and current equations should be derived. Fig. 2 presents the current regulation using a hysteresis current controller which is similarly configured in DSP with the digital current controller. The voltage and current equations can be summarized in Table 1.

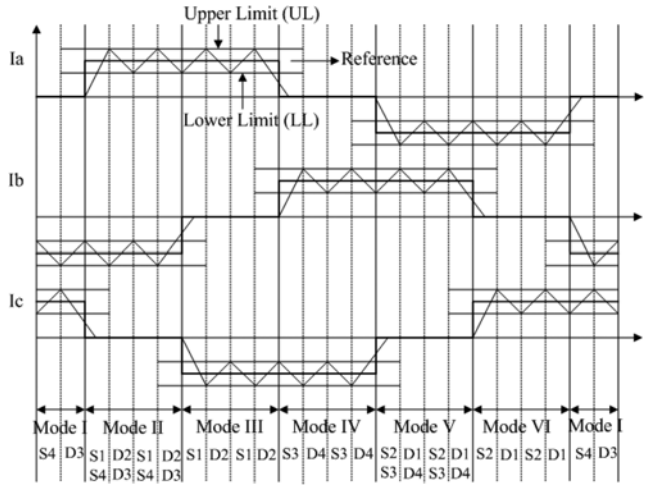

Fig. 2. Detailed current regulation and activated devices.

Table 1. Voltage and Current Equations.

Mode	$di/dt > 0$	$di/dt < 0$
Mode I	$\frac{di_c}{dt} = -\frac{R}{L}i_c + \frac{1}{2L}(V_d - e_{cb})$	$\frac{di_c}{dt} = -\frac{R}{L}i_c - \frac{1}{2L}(V_d + e_{cb})$
Mode II	$\frac{di_a}{dt} = -\frac{R}{L}i_a + \frac{1}{2L}(2V_d - e_{ab})$	$\frac{di_a}{dt} = -\frac{R}{L}i_a - \frac{1}{2L}(2V_d + e_{ab})$
Mode III	$\frac{di_a}{dt} = -\frac{R}{L}i_a + \frac{1}{2L}(V_d - e_{ac})$	$\frac{di_a}{dt} = -\frac{R}{L}i_a - \frac{1}{2L}(V_d + e_{ac})$
Mode IV	$\frac{di_b}{dt} = -\frac{R}{L}i_b + \frac{1}{2L}(V_d - e_{bc})$	$\frac{di_b}{dt} = -\frac{R}{L}i_b - \frac{1}{2L}(V_d + e_{bc})$
Mode V	$\frac{di_b}{dt} = -\frac{R}{L}i_b + \frac{1}{2L}(2V_d - e_{ba})$	$\frac{di_b}{dt} = -\frac{R}{L}i_b - \frac{1}{2L}(2V_d + e_{ba})$
Mode VI	$\frac{di_c}{dt} = -\frac{R}{L}i_c + \frac{1}{2L}(V_d - e_{ca})$	$\frac{di_c}{dt} = -\frac{R}{L}i_c - \frac{1}{2L}(V_d + e_{ca})$

2.2. Flux Reversal Motor Model and Torque Equation Analysis

A six-pole stator and eight-pole variable reluctance rotor of the FRM prototype is presented in Fig. 3. The stator and rotor pole configurations, rotor geometry, magnets, and air gap to obtain a reasonable permeance coefficient value are mainly determined by the performance characteristics of the FRM. As a result, the FRM with the specification in Table 2 has been designed and satisfied the performance and the characteristics of FRM in this paper. The cross section of the FRM can be shown in Fig. 3.

The prototype of FRM has a doubly salient structure in Fig. 3. The drive of FRM is performed by the pwm control with the digital current controller. Also, the switching devices of the drive are the MOSFETs or IGBTs depend-

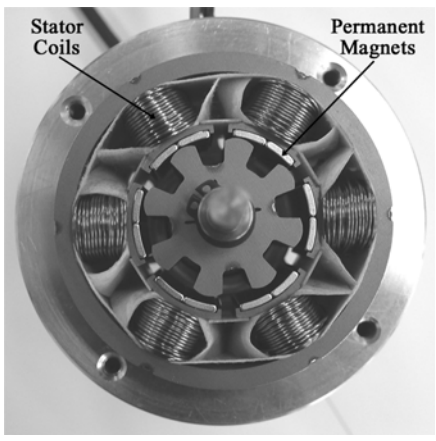

Fig. 3. Configuration of the developed flux reversal motor.

Table 2. Specifications of Flux Reversal Motor.

Section	Item	Value	Unit
Stator	Number of phases	3	
	Number of slots	6	
	Outer diameter	83	mm
	Stack width	35	mm
	Number of turns/phase/pole	70	turns
Rotor	Number of poles	8	
	Outer diameter	40	mm
Magnet	Material	Nd-Fe-B	
	Residual flux density (B_r)	1.15	T
Air-Gap	Mechanical air-gap	0.5	mm

ing on the dc link voltages and switching frequencies. The direct current control scheme is realized according to the position of the rotor in the speed control of FRM.

The self inductance of stator (L) in the FRM is mainly dependent on the rotor position (θ) and the permanent magnet in the stator (λ_{PM}) is related to the variation of air gap flux linkage (λ) as below. This relation can be described as Eq. (1), where 'i' is the stator currents.

$$\lambda(\theta) = \lambda_{PM}(\theta) + L(\theta) \cdot i \tag{1}$$

With the assumption of no saturation in the inductance, the magnetic coenergy (J) can be derived as

$$W = \int \lambda \cdot di = \int \lambda_{PM} \cdot di + \int Li \cdot di = \lambda_{PM}(\theta) \cdot i + \frac{1}{2} Li^2 \tag{2}$$

Therefore, the torque (T) can be obtained as

$$T = \frac{d\lambda_{PM}}{d\theta} \cdot i + \frac{1}{2} \cdot i^2 \cdot \frac{dL}{d\theta} \tag{3}$$

3. Finite Element Analysis and the Experimental Results

3.1. Current and Torque Ripples Analysis of the FRM with pwm inputs

To perform the precise analysis, we used the two-dimensional time-stepped FEM [12]. The simulated phase currents for the 6-switch FRM drive and 4-switch FRM drive using the FEM analysis model are depicted in Fig. 4(a) and (b). The rotor speed is 1500 rpm and the output power is 100W. In the case of the 4-switch FRM drive phase current, in order to compensate the back-EMF current of phase C, phase A and phase B currents should be sensed and controlled independently by a digital PI current controller as mentioned above. In Fig. 4(a) the three phase current waveforms can be shown in a general conventional 6-switch inverter with three digital PI current

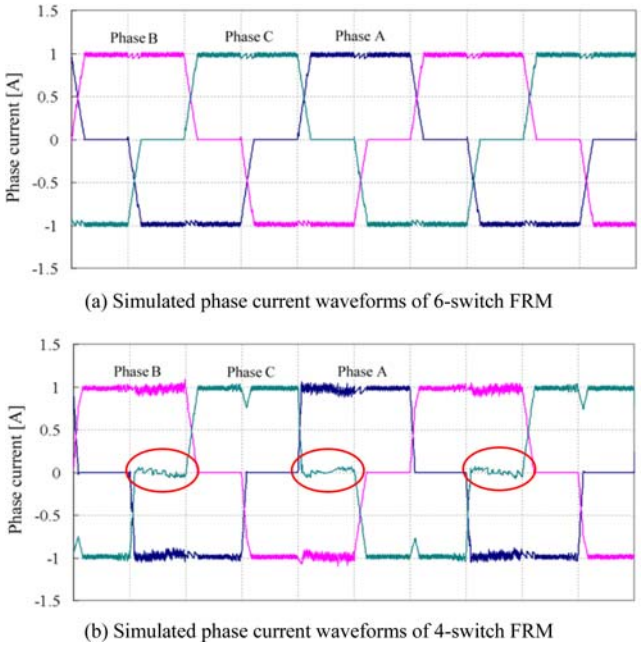

Fig. 4. (Color online) Simulated phase current waveforms using FEM.

controllers. As shown in Fig. 4(a), Fig. 4(b) shows the three phase current waveforms but it has just two digital PI current controller in the 4-switch direct current control scheme, the commutation ripple near zero current of phase B is much higher than the other two phases (phase A and phase B) because it is the uncontrollable phase that is directly connected to the neutral point of the capacitor

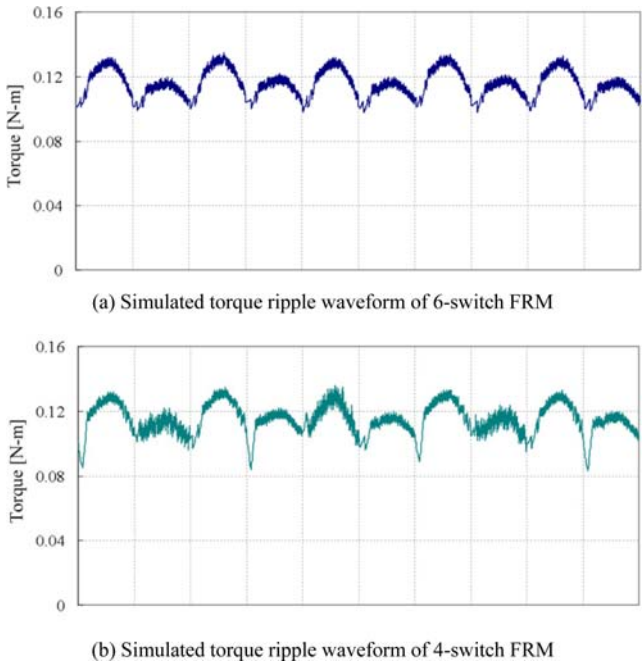

Fig. 5. (Color online) Simulated torque ripple waveforms using FEM.

bank.

The torque ripple waveforms are shown in Figs. 5(a) and (b). Usually it can be easily understood that the 4-switch FRM drive has a higher torque ripple and lower average torque compared with that of the 6-switch FRM drive in the case of the same input voltage, due to the supplying voltage irregularity, the lack of a phase control freedom, and the deeper commutation dip as shown in Fig. 5(b). However, using the voltage-doubler with increasing the switching frequencies of the digital current controller, it can reduce the torque ripples and be similar to that of the 6-switch FRM drive except for a few more ripples in current and output torque. The main reason for this ripple is the restriction of the switching frequency of the inverter topology and the sampling time of the digital current controller. This digital current controller characteristic for the torque ripple is the same as the hysteresis current controller due to same reason on the switching frequency restriction.

3.2. The Experimental Results

In Fig. 6, the experimental configuration of the 4-switch FRM drive is shown. As shown in Fig. 6, the speed of FRM is detected by the encoder with a 1024 pulse, the phase currents of FRM are sensed by the hall C/T and the switching sequence is calculated by the digital controller according to the rotor position that is calculated by the encoder pulse. Also, by use of the error of current reference and current feedback, the digital current controller performs the pwm output duty of the 4-switch FRM drive which is the same as the switching frequency of the 4-switch drive and the digital speed controller makes the current reference of the whole drive system. In Fig. 7, the configuration of the experimental setup is shown.

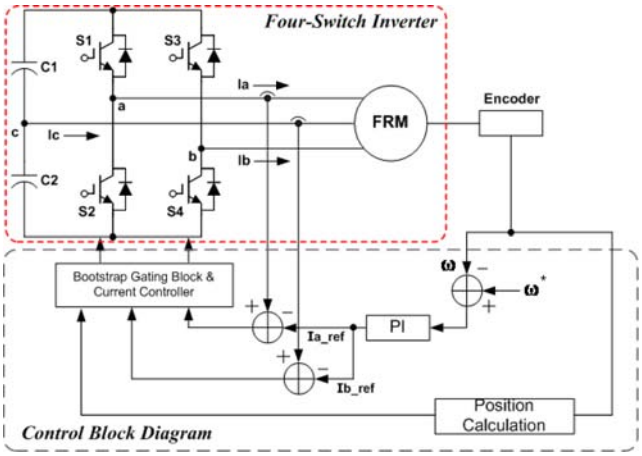

Fig. 6. (Color online) Configuration of the 4-switch FRM driver for experimental results.

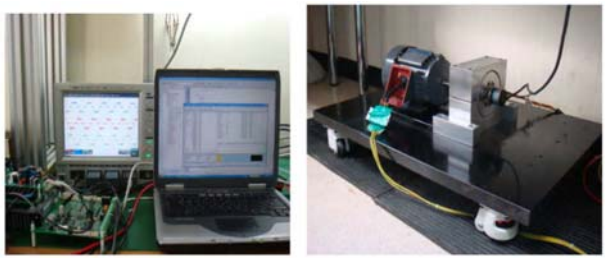

Fig. 7. (Color online) Configuration of the 4-switch FRM driver and Flux Reversal Machine on the test bed for the experimental test.

In Fig. 8, the experimental current waveforms for 6-switch FRM and 4-switch FRM are shown as below. Especially in the 4-switch FRM drive experiment, the commutation ripple of the uncontrollable phase B is higher than that of the other two phases A and C, as is same to the simulation results shown in Fig. 4(b). As a result, shown in Fig. 8, it is verified that the simulated FEM current waveforms are identical to the actual current waveforms, so that they can be utilized as the pwm input data for performance analysis of the 6-switch FRM drive and 4-switch FRM drive.

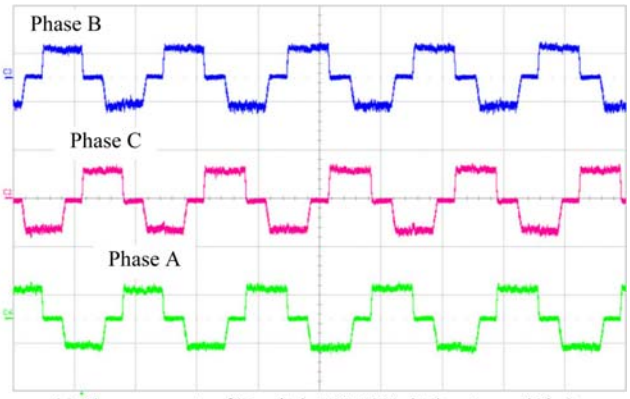

(a) Phase currents of 6-switch FRM (2A / Div., 5msec/Div.)

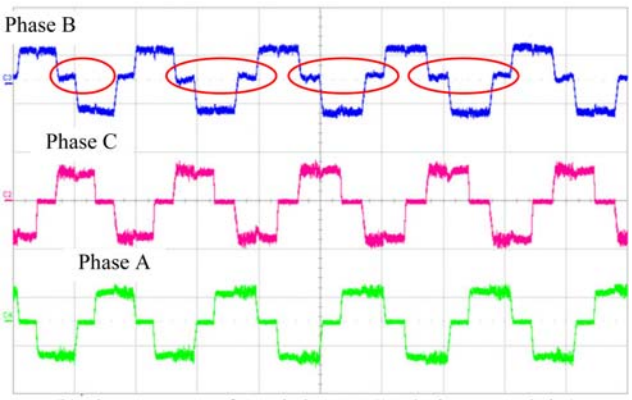

(b) Phase currents of 4-switch FRM (2A / Div., 5msec/Div.)

Fig. 8. (Color online) Experimental phase current waveforms.

3.3. Iron Loss Analysis

The eddy current and the hysteresis losses of the core are calculated from the time variation of the magnetic fields obtained by the FEM with the consideration of the time harmonics [13, 14]. Under this method it is assumed that every relative maximum and relative minimum make a hysteresis loop and the shape of each loop make it identical to the relative maximum and relative minimum of the fundamental hysteresis loop. In addition, if there is a magnetic field having the time harmonics induced to the iron, the hysteresis losses are calculated by the Eq. (5). The eddy current and hysteresis losses of the core W_{ie} and W_{ih} can be calculated as follows:

$$W_{ie} = \frac{K_e D}{2\pi^2} \int_{CORE} \frac{1}{N} \sum_{k=1}^{N} \left\{ \left(\frac{B_r^{k+1} - B_r^k}{\Delta t} \right)^2 + \left(\frac{B_\theta^{k+1} - B_\theta^k}{\Delta t} \right)^2 \right\} dv \quad (4)$$

$$W_{ih} = \frac{K_h D}{T} \sum_{i=1}^{NE} \frac{\Delta V_i}{2} \times \left(\sum_{j=1}^{Npr^i} (B_{mr}^{ij})^2 + \sum_{j=1}^{Np\theta^i} (B_{m\theta}^{ij})^2 \right) \quad (5)$$

Where K_e and K_h are the eddy-current and hysteresis loss coefficient obtained by the Epstein Method. D is the density of the core, N is the number of time steps per time period, Δt is the time interval, ΔV_i is the volume of the ith finite element, B_r, B_θ are the radial and the peripheral components of the flux density, and B_{mr}^{ij}, $B_{m\theta}^{ij}$ are the amplitude of each hysteresis loop.

By using those two equations and the FEM analysis, Fig. 9 shows the comparison of eddy current loss and hysteresis loss of FRM with the 6-switch drive and 4-switch drive. The hysteresis loss in the stator and the rotor is similar in both drive cases. In the stator, however, the eddy current loss of FRM with the 4-switch drive is much larger than that of the 6-switch drive. This can be explained from the fact that the magnetic flux changes quickly under the 4-switch inverter. Therefore, to improve the performance of the FRM with the 4-switch inverter, an advanced PWM control strategy should be developed and implemented.

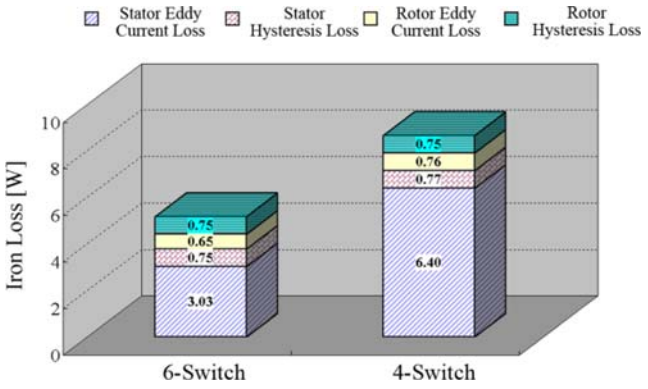

Fig. 9. (Color online) Comparison of eddy current loss and hysteresis loss.

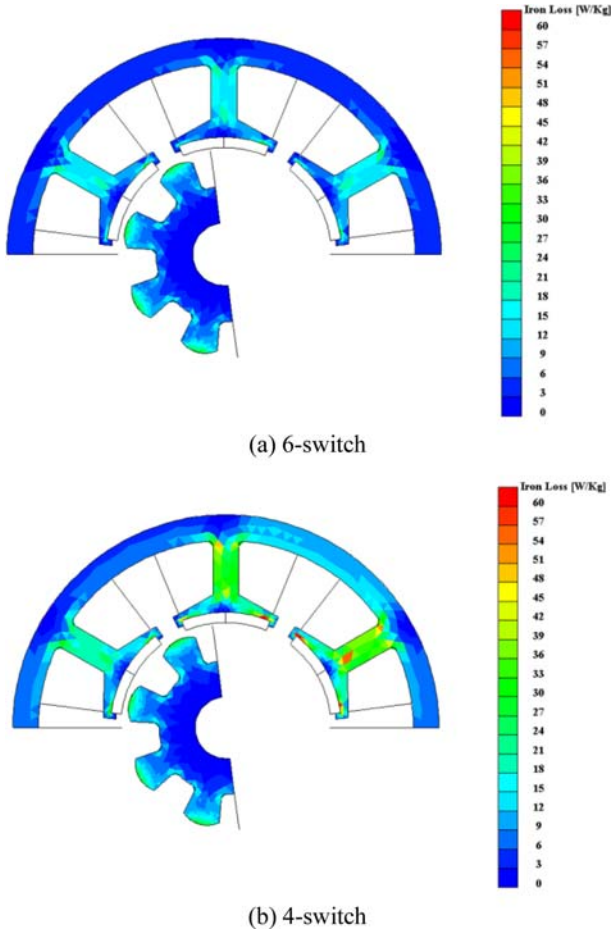

Fig. 10. (Color online) Comparison of iron loss density distribution.

Fig. 10 presents the iron loss distribution of each inverter. From this figure, we can see that the iron loss in the stator is higher in case of the 4-switch.

4. Conclusions

The analysis and characteristic comparison between the 6-switch inverter topology and 4-switch inverter topology for FRM with pulse width modulation inputs has been carried out. For the analysis of the FRM with the two different drive topologies, a 2-dimensional time-stepped voltage source FEM that is taking account of pwm current inputs in the 4-switch and 6-switch drive has been used. Compared to the conventional sinusoidal input to the motor, pwm input reveals the torque ripple, iron losses and mechanical losses. To compare the characteristics between the 6-switch and 4-switch, the prototype FRM is

developed and a DSP installed experimental devices with digital current controller are equipped. As a result, the experimental results with two different drive topologies have been performed. Finally, the comparison of the torque ripple and iron losses with two different inverter topologies are calculated and analyzed in this paper.

From this analysis, this paper shows that the 4-switch drive has approximately 2 times more stator eddy current loss than the 6-switch drive and the other losses of the different two drives are similar. From these characteristics, this paper provides a useful guide to adopt the 4-switch FRM drive compared to the conventional 6-switch FRM drive in regards to the cost and loss view point of applications.

References

[1] K. T. Chau, C. C. Chan, and C. Liu, IEEE Trans. Ind. Electron. **55**, 2246 (2008).
[2] M. Parmar and J. Y. Hung, IEEE Trans. Ind. Electron. **51**, 290 (2004).
[3] M. Morimoto, K. Aiba, A. Hoshino, and M. Fujiwara, IEEE Trans. Ind. Electron. **53**, 415 (2006).
[4] C. Gerada and K. J. Bradley, IEEE Trans. Ind. Electron. **55**, 3300 (2008).
[5] C. Silva, G. Asher, and M. Sumner, IEEE Trans. Ind. Electron. **53**, 373 (2006).
[6] R. P. Deodhar, S. Anderson, I. Boldea, and T. J. E. Miller, IEEE Trans. Ind. Appl. **33**, 925 (1997).
[7] T. H. Kim, K. B. Jang, Y. D. Chun, and J. Lee, IEEE Trans. Magn. **41**, 1916 (2005).
[8] T. H. Kim and J. Lee, IEEE Trans. Magn. **41**, 1956 (2005).
[9] T. H. Kim and J. Lee, IEEE Trans. Magn. **43**, 1725 (2007).
[10] B. K. Lee, T. H. Kim, and M. Ehsani, IEEE Trans. Power Electron. **18**, 164 (2003).
[11] H. S. Kang, T. H. Kim, and B. K. Lee, INTERMAG GN-07, 1190 (2008).
[12] B. K. Lee and T. H. Kim, J. Magnetics **17**, 124 (2012).
[13] K. Yamazaki, IEEE Trans. Magn. **39**, 1460 (2003).
[14] K. B. Jang and T. H. Kim, IEEE Trans. Magn. **41**, 4024 (2005).